Preprints of the 21st IFAC World Congress (Virtual)
Berlin, Germany, July 12-17, 2020

Experimental Comparison of Nonlinear Guidance Laws for Unmanned Aircraft

Nicolas Sedlmair * **Julian Theis** * **Frank Thielecke** *

* *Institute of Aircraft Systems Engineering, Hamburg University of Technology, Hamburg, Germany. (e-mail: {nicolas.sedlmair, julian.theis, frank.thielecke}@tuhh.de).*

Abstract: Two aircraft guidance algorithms from the literature, the Non-Linear Guidance Law (NLGL) and the Nonlinear Differential Geometric Path-Following Guidance Law (NDGPFG), are assessed using a 25 kg unmanned aerobatic aircraft. The paper provides experimental results of the first flight test with the NDGPF. Prior to the real world application, a simulation study is performed to mitigate the risk. For both guidance laws, tracking performance is investigated on a purely kinematic model with unlimited control bandwidth first. Both laws provide superb tracking and the NDGPFG achieves exact path-following, i. e. zero track error. In a second simulation, a high-fidelity model of the aircraft is used. This model includes parasitic dynamics and hence has a finite control bandwidth. In contrast to the results with the purely kinematic model, neither of the algorithms achieves exact path-following with the high-fidelity model. Nevertheless, both guidance laws provide good tracking performance and prove feasible in varying environmental conditions. This observation is finally confirmed in the flight test experiment.

Keywords: flight control, aircraft control, nonlinear control, guidance systems, control application, experimental validation

1. INTRODUCTION

Path-following is a key enabler for increasing autonomy of unmanned aerial vehicles (UAV) and has been extensively studied in the literature, see e. g. Sujit et al. (2014) for a survey. Different nonlinear approaches are used for guiding an aircraft along a desired path. Vector-field-based approaches steer the aircraft towards the path along predefined vector fields, (e. g. Lawrence et al., 2008; de Marina et al., 2017; Nelson et al., 2007). Error-based methods (e. g. Ratnoo et al., 2011) regulate a previously defined error such as heading error or track error. Virtual-target-following approaches guide the aircraft towards a moving point on the path or in a specific direction (e. g. Park, 2012; Lizarraga et al., 2013; Cho et al., 2015). Several approaches within the group of virtual-target-following techniques are investigated in the literature and can also be found in real-world applications. The Non-Linear-Guidance-Law (NLGL) (Park et al., 2004; Park, 2012) is one approach that gained wide attention within the last decade. Its main advantages derive from the so-called *look-ahead effect*. Because the virtual target point is ahead of the vehicle, the shape of the desired path can be incorporated into the guidance law. Moreover, the NLGL is simple to implement and independent of the model. Further, it is able to compensate for unknown wind. Park (2012) used the NLGL to fly aerobatic maneuvers with a small-scale 2.3 kg aircraft.

A derivative from the NLGL is the so-called Nonlinear Differential Geometric Path-Following Guidance Law (NDGPFG) by Cho et al. (2015). Results presented by Cho et al. (2015) show superiority over the NLGL with respect to exact path-tracking, i. e. the track error remains zero throughout the flight. Rather than pursuing a virtual target point, the NDGPFG creates the look-ahead effect by using a *look-ahead angle* to overcome some limitations of the NLGL. Stability analysis for the laws are provided in Park et al. (2007); Deyst (2009); Cho et al. (2015).

The present paper assesses the NDGPFG experimentally. For comparison, an extended version of the NLGL is used. This version was introduced by Sedlmair et al. (2019b) to enable 3D cubic-spline-path-following and was validated in flight tests and simulation studies, see (Sedlmair et al., 2019a). Both algorithms and their respective differences are described in Sec. 2. Section 3 introduces the 25 kg unmanned aerobatic aircraft ULTRA-Extra and a high-fidelity model of the aircraft. In Sec. 4 both guidance laws are investigated in simulations for a 3D cubic-spline-path tracking task. First, a purely kinematic model with unlimited control bandwidth is used. Then, the high-fidelity model with finite control bandwidth is simulated. Finally, flight test experiments are presented in Sec. 5 providing the first experimental validation of the NDGPFG's feasibility for path tracking in real-world application.

2. GUIDANCE LAWS

Both guidance laws investigated within this paper are used as outer-loop controllers providing reference commands for inner-loop flight control laws.

Copyright lies with the authors

2.1 Nonlinear Guidance Law

The basic principle of the NLGL is illustrated in Fig. 1. Denote the aircraft position $P \in \mathbb{R}^3$ and the aircraft velocity $V \in \mathbb{R}^3$ in an inertial reference frame. The aircraft is in close proximity to a path $S(r) : \mathbb{R} \mapsto \mathbb{R}^3$ where r is the arc length along the path. Define the *look-ahead point* $T \in \mathbb{R}^3$ at the intersection of the path $S(r)$ and a sphere with given constant radius $R \in \mathbb{R}_+$ around the aircraft. As the UAV advances, the virtual target point T moves along the path. The difference between the aircraft position and the target point T is $L = P - T$ and the distance $\|L\| = R$ is constant. As shown in Park et al. (2004), R is a tuning parameter that can be chosen, e. g., based on a stability analysis with a linear plant model.

The NLGL computes the acceleration required to align the velocity vector V with L as

$$a_{\text{cmd}} = \frac{2}{\|L\|^2}(V \times L) \times V = \begin{bmatrix} 0 \\ a_{\text{h,cmd}} \\ a_{\text{v,cmd}} \end{bmatrix}, \tag{1}$$

where L and V are expressed in the flight-path coordinate system. Thus, a_{cmd} has no component in the direction of flight. The acceleration commands are always normal to the current velocity vector and correspond to horizontal ($a_{\text{h,cmd}}$) and vertical ($a_{\text{v,cmd}}$) acceleration commands.

One limitation of the NLGL is that exact path-following is only possible for two-dimensional curves of constant curvature. The limitation of the NLGL is best shown using the Frenet-Serret frame. At every point U on $S(r)$, the Frenet-Serret frame forms an orthonormal basis $\{\hat{T}_U, \hat{N}_U, \hat{B}_U\}$ consisting of the unit tangent, normal and binormal vector, see Fig. 2. For a continuously differentiable curve $S(r)$, vector differential equations called the Frenet-Serret formulas describe its kinematic characteristics. As shown in Cho et al. (2015), the acceleration required to move exactly along the curve $S(r)$ starting from any point U on that curve is

$$a_U = \|\dot{V}\|\,\hat{T}_U + \kappa_U \|V\|^2\,\hat{N}_U. \tag{2}$$

Here, κ_U is the curvature of the path at the point U. Equation (2) implies that the binormal acceleration must vanish and that the normal acceleration must equal $\kappa_U \|V\|^2$. An equivalent formulation for this is

$$\langle a_{U,\text{cmd}}, \hat{N}_U \rangle = \kappa_U \|V\|^2, \tag{3a}$$
$$\langle a_{U,\text{cmd}}, \hat{B}_U \rangle = 0, \tag{3b}$$

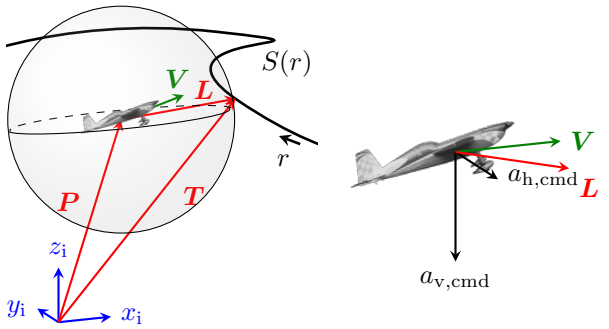

Fig. 1. Target point definition and acceleration to rotate the velocity vector towards the target point.

where, $\langle \cdot, \cdot \rangle$ denotes the scalar product. Assume now that an aircraft is on the path (i. e. $U = P$) and that its velocity vector V is aligned with the tangent vector $\hat{T}_U$. The acceleration command a_{cmd} calculated from (1) lies within the (V, L)-plane and hence has a component in the direction of $\hat{B}$, see Fig. 2. Thus, the NLGL does not satisfy condition (3b) unless $S(r)$ is a 2-D curve. Exact path-following of 3D curves with varying curvature is hence impossible.

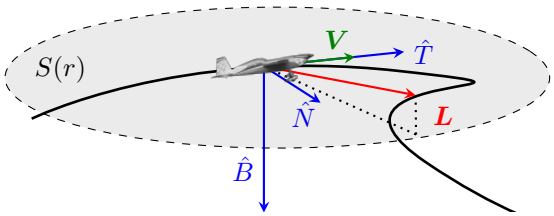

Fig. 2. Frenet-Serret Frame, limitation of the NLGL tracking 3D curves.

2.2 Nonlinear Differential Geometric Guidance Law

The NDGPFG as described by Cho et al. (2015) overcomes the limitation of the NLGL. The NDGPFG incorporates the known curvature of the desired path and allows, in principle, exact path-following. An important difference to the original NLGL is that the NDGPFG uses a *look-ahead angle* instead of a *look-ahead point*. Its look-ahead vector $\hat{L} \neq L$ is a function of four parameters $(e, k, \kappa_F, \delta_{BL})$ and $\|\hat{L}\|$ is not fixed. The NDGPFG calculates the acceleration command as

$$a_{\text{cmd}} = k\,(V \times \hat{L}) \times V = \begin{bmatrix} 0 \\ a_{\text{h,cmd}} \\ a_{\text{v,cmd}} \end{bmatrix}, \tag{4}$$

where $\hat{L}$ and V are again expressed in the flight-path coordinate system. The parameter $k > 0$ can be used as a tuning knob and affects the aggressiveness of the guidance law. Further, it sets a maximum bound for the acceleration command as $\|a_{\text{cmd}}\| \leq k\|V^2\|$. Considering the curvature of $S(r)$, k should be selected such that $k \geq \max_r |\kappa_{S(r)}|$. The parameter $\delta_{BL} > 0$ can be considered as an additional tuning knob affecting the steepness of the approach towards the path. The parameters e and κ_F depend on the closest projection point F, i. e., the point on $S(r)$ that is closest to P in the Euclidean norm. The tracking error is $e = \|P - F\|$ and κ_F is the curvature of the path at F. Thus, finding a unique F is necessary to compute the look-ahead vector $\hat{L}$ and the acceleration a_{cmd}. For further details, the reader is referred directly to Cho et al. (2015).

3. ULTRA-EXTRA AIRCRAFT AND CONTROLLER ARCHITECTURE

The ULTRA-Extra, depicted in Fig. 3, is an unmanned aerobatic aircraft with a total mass of 24.6 kg and a wingspan of 3.10 m. It is equipped with an electric propulsion system and high quality avionics. A real-time computer hosts GNC applications, processes measurements, and issues control outputs to the servos. Acceleration and rate measurements are provided by an industry-grade navigation platform. Dual-antennas determine heading and

GPS position. An accuracy of up to 0.02 m is possible through the use of Differential GPS correction. A five-hole-probe, developed in-house, measures air data such as angle of attack, angle of sideslip, static air pressure, airspeed, and air temperature. Calibration was done based on data gathered in an extensive wind tunnel campaign (Niemann et al., 2014).

Fig. 3. Flight test aircraft ULTRA-Extra.

3.1 Controller Architecture

Both guidance laws described in Sec. 2 require inner-loop controllers that track the commanded accelerations $a_{\mathrm{h,cmd}}$ and $a_{\mathrm{v,cmd}}$. The ULTRA-Extra employs a cascaded single-input-single-output control architecture where longitudinal and lateral-directional control are separated, see Fig. 4. The horizontal acceleration command can be translated into a reference for the bank angle controller. The vertical acceleration command is transformed into the body-fixed coordinate frame and is provided to the vertical acceleration controller as a reference, cf. Sedlmair et al. (2019b). Airspeed is maintained by a conventional autothrottle. The sideslip angle is controlled to zero throughout the flight to achieve an aerodynamically clean flight. All controller gains are scheduled with airspeed to account for varying dynamics.

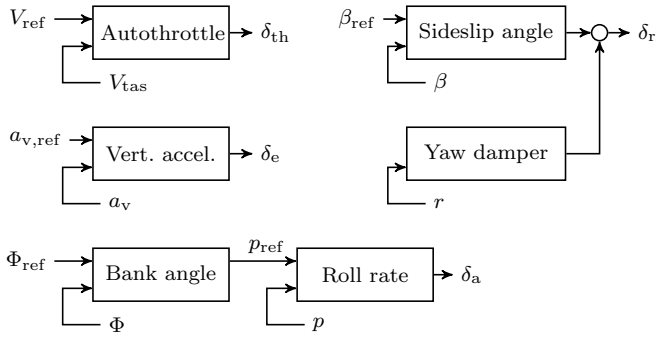

Fig. 4. Cascaded basic flight control law architecture.

3.2 Simulation Model

For simulation studies, a high-fidelity nonlinear model of the ULTRA-Extra aircraft is derived. It includes a nonlinear aerodynamics model, accurately identified in an extensive flight test campaign with a total of 148 identification maneuvers (Sedlmair et al., 2019b). A model of the electric propulsion system computes the moment at the support and the thrust for a wide range of inflows at the propeller and throttle positions. It is based on data obtained in a wind tunnel campaign. The dynamics of the control surface servos where identified on the component level and the model acknowledges time delays and control surface backlash. The moment of inertia tensor was determined through experiments. Sensors are modeled with their measured noise characteristics. Further, signal filtering as well as computational and communication delays are included. Wind and atmospheric turbulence are simulated according to MIL-F-8785C.

4. FLIGHT TEST SIMULATION

Cho et al. (2015) make two major assumptions in the derivation of their NDGPFG: 1) A fixed-wing aircraft is approximated as a 3-DoF point mass, and 2) the inner-loop controllers track the commanded accelerations exactly and instantaneously, i. e., no actuator dynamics or other lags are present. In a first simulation within this work, the results of Cho et al. (2015) are confirmed using a 3-DoF model in accordance with their assumptions. In a second step, the complete nonlinear aircraft model as described in Sec. 3.2 is used. For both simulation studies as well as for the flight tests presented in Sec. 5, a common test scenario is defined.

4.1 Test Scenario

The test scenario is a 3D cubic spline-path-following task similar to the scenario described in Cho et al. (2015). The desired path within the scenario connects nine waypoints, see Tab. 1. The 3D spline-path-following algorithm outlined in Sedlmair et al. (2019b) is used. The algorithm is extended such that it also computes the closest projection point F and the curvature of the path κ_F at F, as required by the NDGPFG. The commanded airspeed throughout the flight is $V_{\mathrm{A}} = 25\,\mathrm{m/s}$. Performance is measured by the cost function $J = \frac{1}{t_{\mathrm{f}}-t_0}\int_{t_0}^{t_{\mathrm{f}}} \|e\|\,\mathrm{d}t$, i. e., the mean track error.

Table 1. Waypoints ([North, East, Altitude]) used for path definition.

No.	Position in m	No.	Position in m	No.	Position in m
1	$[110, -40, 130]$	4	$[-97, 422, 130]$	7	$[551, 122, 180]$
2	$[-57, 72, 130]$	5	$[203, 480, 110]$	8	$[511, -100, 160]$
3	$[-157, 272, 110]$	6	$[314, 335, 160]$	9	$[333, -178, 130]$

4.2 Simulation 1: Point Mass Acceleration

Assumption 1) of Cho et al. (2015) means that the motion of the aircraft is independent of its attitude and that moments are neglected. Thus, turning rates as well as pitch and bank angle are held constant at zero. Assumption 2) states that the commanded accelerations computed by the guidance laws are directly applied to the center of gravity of the aircraft model. Therefore, servo dynamics, sensor dynamics, filter dynamics, and time delays are neglected. As such, only the basic kinematics of a point in the 3D space remain.

In the first simulation run, the NLGL is tested and acceleration commands are computed according to Eq. (1).

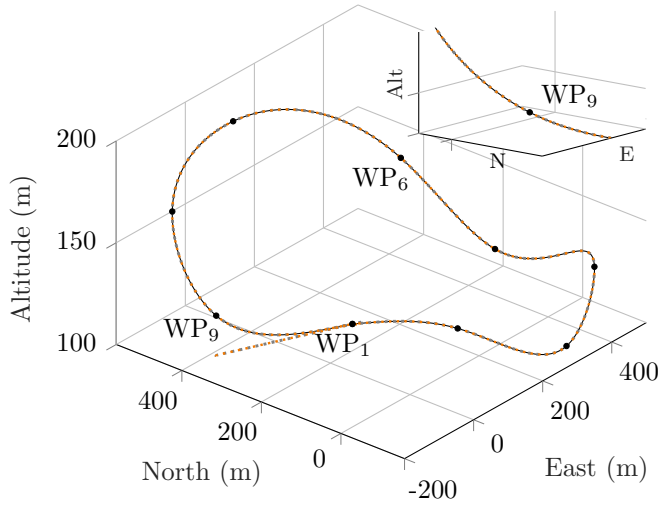

Fig. 5. Simulation with the kinematic model: Reference-path (——) and simulation results for the NLGL (·····) and the NDGPFG (·····).

At initialization, the aircraft is located 20 m below the last waypoint (WP_9) while headed in a direction perpendicular to the desired track. Its flight-path velocity is $V = 25\,\mathrm{m/s}$. The aircraft approaches the first waypoint (WP_1) until the path comes into the range R. Once a target point T is found, the NLGL guides the aircraft along the path. In the second simulation, the NLGL is used to approach the first waypoint and authority is switched to the NDGPFG once the aircraft is close enough to calculate a closest projection point F and the track error e. Then, acceleration commands are computed according to Eq. (4). Little guidance is provided by Cho et al. (2015) on how to choose the design parameters for the NDGPFG. Hence, controller parameters for both guidance laws are tuned iteratively in order to minimize the performance index J. For the NLGL, the sphere's radius is chosen as $R = 3\,\mathrm{m}$. For the NDGPFG, tuning parameters are chosen as $k = 0.2$ and $\delta_{BL} = 1\,\mathrm{m}$.

Investigating Fig. 5 proves tight tracking capabilities of the NLGL and the NDGPFG with the kinematic model. The performance of the controllers is further analyzed by comparing the track error over time, see Fig. 6. After an initial error at $t \approx 11\,\mathrm{s}$, the NDGPFG proves its exact path-following capabilities as the track error is reduced to zero throughout the path. This is not entirely the case for the NLGL, as isolated peaks with $e \neq 0$ occur at the waypoints. These peaks result when the spline-path following algorithm switches the currently active spline-segment because the aircraft is sufficiently close to the waypoint, see Sedlmair et al. (2019b) for further details. The duration of the peaks is short and the magnitudes are low. Moreover, the track error in-between the waypoints is zero, leading to a small mean error of $J_{\mathrm{NLGL}} = 0.003\,\mathrm{m}$. This error would be negligible for any practical application as it is significantly less than the GPS accuracy. As $J_{\mathrm{NDGPFG}} = 0\,\mathrm{m}$, both guidance laws provide very similar performance under the given assumptions. Note, however, that assumptions 1) and 2) allow an infinite control bandwidth as accelerations are applied instantaneously. Thus, the parameters are likely to be too aggressive for actual application.

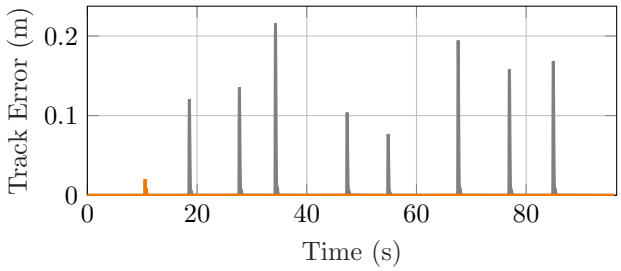

Fig. 6. Simulation with the kinematic model: Track error with the NLGL (——) and the NDGPFG (——).

4.3 Simulation 2: Full Model

For the second simulation, the full high-fidelity model of the ULTRA-Extra is used, including servo dynamics, sensor dynamics, filter dynamics, and time delays. Acceleration commands computed by the guidance laws are now passed as references to the flight control laws as depicted in Fig. 4. First, the controller parameters from the simulation with the kinematic model are applied. As could be expected, unstable behavior is observed because the full model has a finite bandwidth and the controller parameters are too aggressive. Hence, retuning of both guidance laws is necessary in order to apply them in flight test experiments. Parameters are now selected based on simulations with the high-fidelity model. That is, flight-path-following is simulated for varying environmental conditions and controller parameters. For the NLGL, $R \in [30\,\mathrm{m}, 70\,\mathrm{m}]$ is considered. The NDGPFG is evaluated for $k \in [0.03, 0.1]$ and $\delta_{BL} \in [30\,\mathrm{m}, 100\,\mathrm{m}]$. The tuning objective is, again, minimizing the mean tracking error, while avoiding oscillations around the reference path. This leads to a constant sphere radius $R = 50\,\mathrm{m}$ for the NLGL. Note that this value also proved its performance in previous flight tests (Sedlmair et al., 2019b). For the NDGPFG, choosing $k = 0.062$ and $\delta_{BL} = 50\,\mathrm{m}$ gives a good compromise between low mean track error and oscillatory behavior.

Subsequently, simulation results for these parameters are presented. The simulation includes wind conditions that closely resemble the wind measured in the flight test experiment discussed in Sec. 5. Figure 7 depicts the wind's influence on the flight-path velocity with mean wind speed set to $\bar{V}_W = 5.6\,\mathrm{m/s}$ and a mean direction of $\bar{\chi}_W \approx 89°$. Note that both guidance laws account for varying flight-path velocity, see Eqs. (1) and (4). Hence, their path-following capabilities are independent of wind. Dryden turbulence is added to get a more realistic situation.

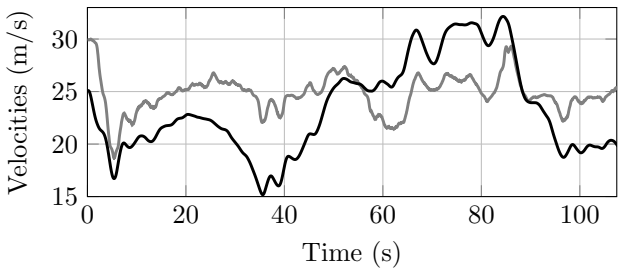

Fig. 7. Simulation with the high-fidelity model: Flight-path velocity V (——) and airspeed V_{A} (——).

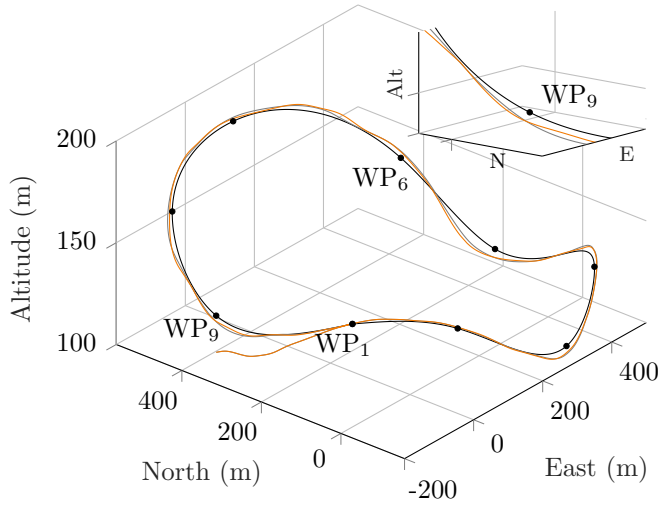

Fig. 8. Simulation with the high-fidelity model: Reference-path (—) and simulation results for the NLGL (—) and the NDGPFG (—).

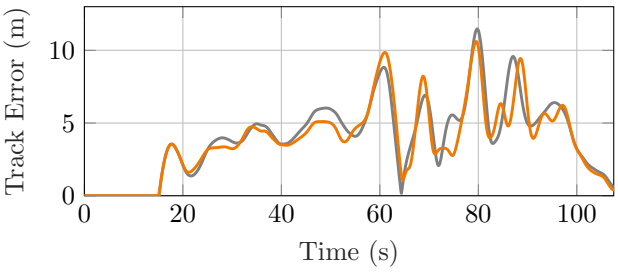

Fig. 9. Simulation with the high-fidelity model: Track error with the NLGL (—) and the NDGPFG (—).

Under these conditions, both guidance laws achieve 3D spline-path-following as can be seen in Fig. 8. Figure 9 shows the track error from initialization at $t_0 = 0\,\mathrm{s}$ until the path is completed. By comparing the track errors of Figs. 6 and 9, significant differences can be observed. In the simulation with the high-fidelity model, none of the guidance laws achieves exact path-following as $e \neq 0$ throughout the entire path. The NDGPFG achieves marginally higher precision as can be concluded by comparing the performance indices $J_{\mathrm{NLGL}} = 4.65\,\mathrm{m}$ and $J_{\mathrm{NDGPFG}} = 4.45\,\mathrm{m}$. For the given 3,1 m wingspan, 25 kg aircraft and speeds of up to 115 km/h, these results are deemed good.

5. FLIGHT TEST EXPERIMENTS

Flight test experiments are performed on the same cubic spline-path as in Sec. 4. During the experiment, wind with a mean speed of $\bar{V}_W \approx 5.6\,\mathrm{m/s}$ and a mean direction of $\bar{\chi}_W \approx 89°$ was measured. The results, shown in Fig. 10, prove the path-following capabilities of both guidance laws in a real world experiment. In the beginning, the safety pilot steers the aircraft close to the first waypoint and the path-following algorithm is engaged. Firstly, the NLGL guides the aircraft along the path for approximately 280 s. After completing three consecutive circuits with the NLGL, authority is switched to the NDGPFG. Again, three consecutive circuits are completed.

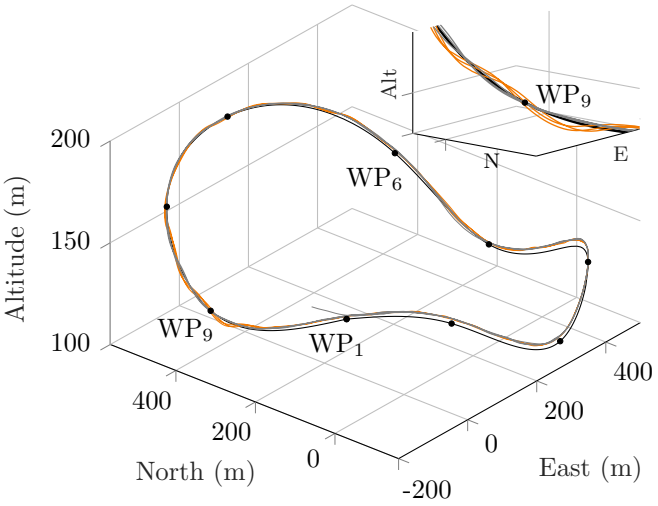

Fig. 10. Flight test results: Reference-path (—) and actual flight path with the NLGL (—) and the NDGPFG (—).

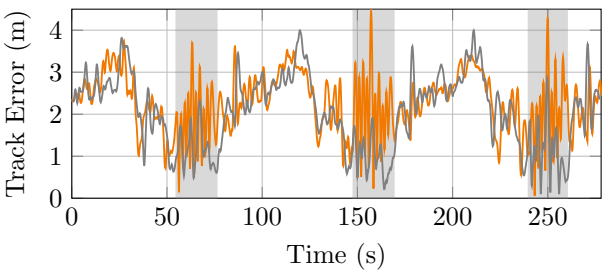

Fig. 11. Flight test results: Comparison of track error over time, NLGL (—) and NDGPFG (—).

Figure 11 compares the track error over time and Fig. 12 depicts the relative cumulative time with respect to the track error. Both figures reveal that the two guidance laws' precision is very similar. As could be expected from the full model simulations, none of them achieves exact path-following. However, the path tracking accuracy for both guidance laws is actually higher in the flight test experiment than with the full model simulation. In fact, the performance indices are more than halved as $J_{\mathrm{NLGL}} = 2.06\,\mathrm{m}$ and $J_{\mathrm{NDGPFG}} = 2.27\,\mathrm{m}$. The track error is less than 2 m for 44 % of the time with the NLGL and 35 % of the time with the NDGPFG. Moreover, the maximum track errors are significantly lower in the flight test compared to the simulation; 3.99 m for the NLGL and 4.44 m for the NDGPFG.

Little discrepancies between both guidance laws appear within the time spans highlighted in Fig. 11. Within these 20 s slices, the aircraft flies between WP_6 and WP_9. Slight oscillatory behavior occurs with the NDGPFG during that particular part of the path, see the inset in Fig. 10. It can be linked to the presence of tailwind as can be concluded by comparing the flight-path velocity V and the measured airspeed V_{A} in Fig. 13. This behavior can also be observed in the simulation with the full model, see Figs. 7 and 8. Altogether, the flight test experiments are in good agreement with the results from the simulation of the high-fidelity model.

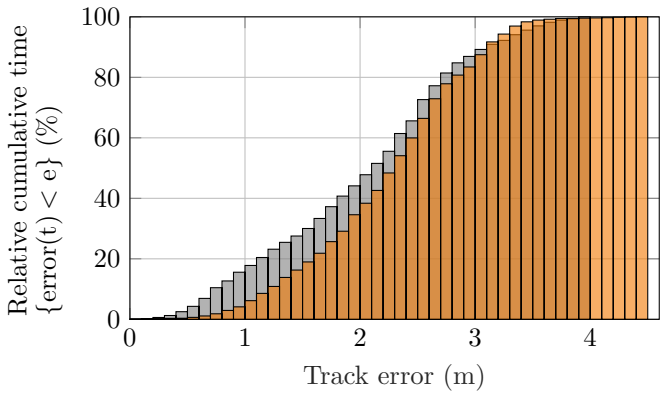

Fig. 12. Flight test results: Comparison of track error, NLGL ( ) and NDGPFG ( ).

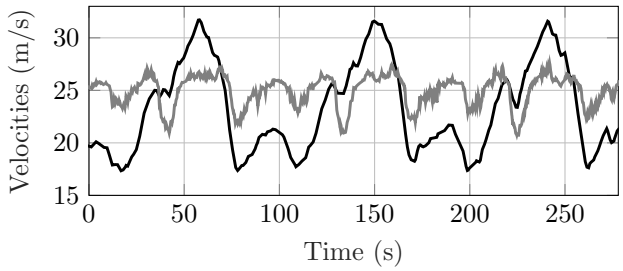

Fig. 13. Flight test results: Flight-path velocity V (——) and airspeed V_A (——).

6. CONCLUSION

Two look-ahead-based nonlinear guidance laws from the literature, the NLGL of Park et al. (2004) and the NDGPFG of Cho et al. (2015) are experimentally validated in flight tests using an aerobatic aircraft. To mitigate the risk, both guidance laws are investigated in simulations. First, a purely kinematic model of the aircraft is simulated and controller outputs are instantaneously applied to a point mass. Under these circumstances, the controlled system has an unlimited bandwidth and the controller parameters are tuned as aggressive as possible to minimize track error. For the 3D cubic-spline-path under consideration, both guidance laws prove feasible and show very similar performance. The NDGPFG provides exact path-following, i. e. zero track error. With the NLGL, a track error negligible for any practical application is observed. In a second simulation, a nonlinear high-fidelity model of the aircraft with a realistic finite bandwidth is used. To avoid instability, retuning of the controllers is necessary. With adopted controller parameters, simulations with the high-fidelity model show good path-following capabilities for both guidance laws in varying environmental conditions. Neither of the laws achieves exact path-following as the finite bandwidth sets limits to the controller gains. Nevertheless, encouraged by the simulations, flight test experiments are performed for validation. For both guidance laws tight tracking performance is observed under real world circumstances with even better results compared to the high-fidelity simulations. In conclusion, both guidance algorithms prove suitable for high-precision tracking tasks with the considered unmanned aircraft.

REFERENCES

Cho, N., Kim, Y., and Park, S. (2015). Three-dimensional nonlinear differential geometric path-following guidance law. *J. Guid., Control, Dyn.*, 38(12), 2366–2385. doi: 10.2514/1.G001060.

de Marina, H.G., Kapitanyuk, Y.A., Bronz, M., Hattenberger, G., and Cao, M. (2017). Guidance algorithm for smooth trajectory tracking of a fixed wing UAV flying in wind flows. In *2017 IEEE Int. Conf. Robotics Automation*. doi:10.1109/icra.2017.7989674.

Deyst, J. (2009). The direct construction of lyapunov functions for nonlinear systems. In *AIAA Guid., Navigation, Control Conf.* doi:10.2514/6.2009-6274. Paper No. 2009-6274.

Lawrence, D., Frew, E., and Pisano, W. (2008). Lyapunov vector fields for autonomous unmanned aircraft flight control. *J. Guid., Control, Dyn.*, 31(5), 1220–1229. doi: 10.2514/1.34896.

Lizarraga, M., Curry, R., and Elkaim, G.H. (2013). Flight test results for an improved line of sight guidance law for UAVs. In *American Control Conf.* doi: 10.1109/acc.2013.6579937.

Nelson, D.R., Barber, D.B., McLain, T.W., and Beard, R.W. (2007). Vector field path following for miniature air vehicles. *IEEE Trans. Robotics*, 23(3), 519–529. doi: 10.1109/tro.2007.898976.

Niemann, C., Montel, M., and Thielecke, F. (2014). Development of an air data system for an unmanned research aircraft. In *Deutscher Luft- und Raumfahrtkongress*.

Park, S. (2012). Autonomous aerobatics on commanded path. *Aerospace Science and Technology*, 22(1), 64–74.

Park, S., Deyst, J., and How, J. (2004). A new nonlinear guidance logic for trajectory tracking. In *AIAA Guid., Navigation, Control Conf.* American Institute of Aeronautics and Astronautics. doi:10.2514/6.2004-4900.

Park, S., Deyst, J., and How, J.P. (2007). Performance and lyapunov stability of a nonlinear path following guidance method. *J. Guid., Control, Dyn.*, 30(6), 1718–1728. doi: 10.2514/1.28957.

Ratnoo, A., Sujit, P.B., and Kothari, M. (2011). Adaptive optimal path following for high wind flights. *IFAC Proceedings Volumes*, 44(1), 12985–12990. doi: 10.3182/20110828-6-IT-1002.03720.

Sedlmair, N., Theis, J., and Thielecke, F. (2019a). Automatic three-point landing of a UAV with H_∞-control in $\mathcal{D}$-implementation. *IFAC-PapersOnLine*, 52(12), 316–321. doi:10.1016/j.ifacol.2019.11.262.

Sedlmair, N., Theis, J., and Thielecke, F. (2019b). Design and experimental validation of UAV control laws – 3D spline-path-following and easy-handling remote control. In *5th CEAS Conf. Guid., Navigation, Control*.

Sujit, P.B., Saripalli, S., and Sousa, J.B. (2014). Unmanned aerial vehicle path following: A survey and analysis of algorithms for fixed-wing unmanned aerial vehicles. *IEEE Control Syst. Mag.*, 34(1), 42–59. doi: 10.1109/MCS.2013.2287568.